ChemComm

COMMUNICATION

View Article Online
View Journal | View Issue

Check for updates

Cite this: *Chem. Commun.*, 2024, **60**, 6031

Received 20th March 2024,
Accepted 15th May 2024

DOI: 10.1039/d4cc01280a

rsc.li/chemcomm

Published on 15 mai 2024. Downloaded on 15.11.2025 00:31:20.

Prevention of ion migration in lead halide perovskites upon plugging the anion vacancies with PbSe islands†

Swati Khurana, Priyesh Yadav, Priyadharsini Natesan, Md Samim Hassan, Deepak Kumar Pradhan and Sameer Sapra *

To circumvent the issue of halide ion exchange in perovskites, we have decorated $CsPbBr_3$ and $CsPbI_3$ nanocrystals with different sized PbSe nanoparticles and demonstrated that it effectively prevents anion exchange reaction in $CsPbBr_3$/$CsPbI_3$ nanoheterostructures (NHSs) as a consequence of halide vacancy passivation by the more covalent selenide anion.

Heterostructures based on different halide perovskite nanocrystals (NCs) have attracted a lot of attention in recent years owing to their use in diverse optoelectronic applications.[1–10] Importantly, the interface between different perovskite layers plays an essential role in determining the performance of optoelectronic devices.[11–16] However, the ease of halide ion migration is critical towards fabrication of all perovskite based tandem optoelectronic devices.[17–26] When two metal halide perovskites (MHPs) of different halide composition are brought in direct contact, rapid diffusion of halide ions occurs, commonly referred to as anion exchange reactions, resulting in the formation of mixed-halide alloys instead of well-defined interfaces.[20,25,27,28] Anion exchange reactions are highly spontaneous in nature and originate due to the low thermodynamic barrier of mixing of different halide ions.[29,30] Moreover, within MHP NCs, anion exchange reactions are further facilitated by the removal of halide ions from the perovskite surface under light exposure and other environmental stresses.[31] To suppress the ion migration in perovskite/perovskite tandem structure, it is quintessential to effectively passivate the halide vacancies through appropriate strategies. Notably, several studies in the literature have described the inhibition of anion exchange either through perovskite capping or the implementation of an ion-blocking layer.[32–35] Buonsanti *et al.* reported the use of alumina shell on perovskite surface which leads to the prevention of ion migration.[35] In a recent study, Blackburn *et al.* showcased the effective use of single-layer graphene inserted between the metal halide perovskite layers to prevent ion diffusion.[36] Kamat and coworkers employed $PbSO_4$-oleate capping on perovskite, which effectively inhibits ion exchange.[37] Balakrishna's group inhibited the halide ion exchange in tandem devices *via* passivating the perovskite's defects using polyvinylpyrrolidone[38] while Santra's group prevented the ion migration at the interfaces of $CsPbBr_3$–$CsPbI_3$ using an ultrathin alumina shell.[39] In this context, utilizing metal chalcogenides for plugging halide vacancies can serve as a potential strategy to prevent the migration of halide ions due to the highly covalent nature of the Pb–chalcogen bond that renders it stable. Recently, a few studies discussed about the passivation of surface defects of halide perovskites *via* NHSs formation with PbE (E = S, Se).[40–44] These NHSs show excellent performance in photovoltaic applications owing to their enhanced stability under ambient conditions.[40,43] However, to the best of our knowledge, the utilization of lead chalcogenide passivation to effectively suppress halide ion exchange in perovskite/perovskite NHSs has not been explored yet. Here we demonstrate PbSe nanoparticles (NPs) decorated over the surface of MHPs greatly passivate the surface defects of $CsPbBr_3$ as well as $CsPbI_3$ NCs. As a result of halide passivation, ion exchange reaction is suppressed significantly in PbSe decorated $CsPbBr_3$/$CsPbI_3$ NHSs, irrespective of the size of the PbSe islands. We observe discrete absorption and photoluminescence (PL) features in PbSe–$CsPbBr_3$/PbSe–$CsPbI_3$ NHSs, as that of isolated $CsPbBr_3$ and $CsPbI_3$ NCs. Whereas, in case of pristine $CsPbBr_3$/$CsPbI_3$ NHSs without PbSe, rapid mixing of halides take place. Moreover, we do not observe any change in the PL emission peaks in PbSe decorated NHSs for over a period of six months under ambient conditions and even upon thermal annealing. Furthermore, we have fabricated phosphor converted light emitting diodes (pc-LED), which show warm white luminescence indicating the retention of the $CsPbBr_3$ and $CsPbI_3$ structures. Our approach opens possibilities for designing novel perovskite/perovskite heterostructures,

Department of Chemistry, Indian Institute of Technology Delhi, Hauz Khas, New Delhi 110016, India. E-mail: sapra@chemistry.iitd.ac.in

† Electronic supplementary information (ESI) available. See DOI: https://doi.org/10.1039/d4cc01280a

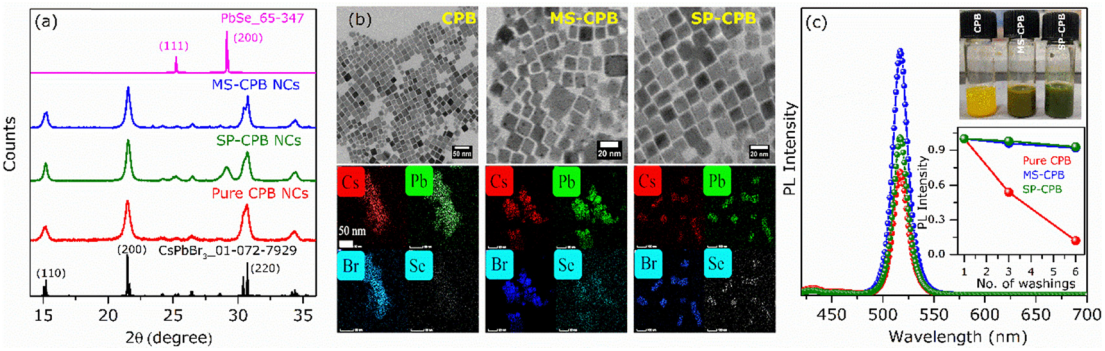

Fig. 1 (a) PXRD pattern for pristine CPB, MS-CPB, and SP-CPB along with their reference patterns; (b) TEM images and STEM elemental mapping for CPB, SP-CPB, and MS-CPB; (c) PL spectra of CPB, SP-CPB, and MS-CPB along with their photographs in day light; inset: comparison of PL stability of CPB, SP-CPB, and MS-CPB after multiple washings with ethyl acetate.

Published on 15 mai 2024. Downloaded on 15.11.2025 00:31:20.

enabling enhanced control over optoelectronic properties in various photonic device applications.

$CsPbBr_3$–PbSe NCs were synthesized utilizing *in situ* colloidal hot injection methods (i) using $MoSe_2$ nanosheets (NSs) and (ii) Se powder as two different source of selenium precursors, reported recently from our group.[44,45] Detailed synthesis methodology is discussed in Experimental Section. For the sake of simplicity, the NCs synthesized from $MoSe_2$ and Se powder are abbreviated MS-CPB and SP-CPB, respectively. Fig. 1a shows the powder X-ray diffraction (PXRD) pattern of $CsPbBr_3$ (CPB) NCs and SP/MS-CPB along with the reference pattern for bulk $CsPbBr_3$ and PbSe, which shows the presence of lattice planes corresponding to both CPB and PbSe in SP/MS-CPB. Transmission electron microscopy (TEM) images of CPB and SP/MS-CPB are shown in Fig. 1b, and their size distribution is shown in Fig. S1 in ESI.† Notably, cubic morphology of CPB remains intact in SP/MS-CPB NCs, accompanied by the presence of small black dots decorating the surface of the CPB NCs, attributed to the presence of PbSe NPs.[44,46] It is interesting to note that in case of SP-CPB, larger sized PbSe islands are formed, while in case of MS-CPB, smaller sized PbSe islands are formed, as can be seen from the histograms in Fig. S1d and e (ESI†), respectively. We establish the presence of PbSe in the SP/MS-CPB through elemental mapping with scanning transmission electron microscopy (STEM)-energy-dispersive X-ray (EDX) spectroscopy as shown in Fig. 1b.[46] A significant increase in the PL intensity is observed in SP/MS-CPB compared to pristine NCs as shown in Fig. 1c, suggesting incorporation of PbSe passivates the surface defects of CPB by filling the halide vacancies.[46] Nonetheless, it is a well-known fact that in pristine halide perovskites, halide vacancies are further created under light exposure and other environmental stresses, facilitated by the detachment of surface halide in the form of oleylammonium halide.[39] Since halide vacancies facilitate anion migration, effective sealing of these vacancies and preventing their further formation during device operation would significantly impede halide ion migration. To ensure effective passivation of halide vacancies in SP/MS-CPB, we subjected the NCs to multiple washings using the antisolvent ethyl acetate. While the PL intensity of pristine CPB drops by up to 50% after three washes, that of SP/MS-CPB only experience a modest reduction of about 10%, as illustrated in Fig. 1c (inset). This is attributed to the removal of surface bromide ions in the form of oleylammonium bromide, which creates more defects in NCs upon washing with antisolvent.[39] The relatively minor reduction in PL intensity observed in SP/MS-CPB suggests that the surface bromide remains largely intact indicating PbSe effectively plugs the halide ion vacancies of $CsPbBr_3$ and offers protection from the external environment under ambient conditions.[43] In PbSe decorated halide perovskite NCs, as the halide vacancies are not created under harsh experimental conditions, we believe that these vacancies are unlikely to form during device operation. Using a similar reaction scheme, we also synthesized PbSe decorated $CsPbI_3$ NCs using $MoSe_2$ NSs and selenium powder, which we are denoting as MS-CPI and SP-CPI, respectively. PXRD pattern of pure $CsPbI_3$ (CPI) NCs and SP/MS-CPI, and their corresponding TEM images are shown in Fig. S2 (ESI†). We now show the utilization of these PbSe decorated $CsPbX_3$ NCs to study the influence of PbSe decoration on ion migration within $CsPbBr_3$/$CsPbI_3$ (CPB/CPI) NHSs. All the measurements were conducted on thin films on a glass substrate. For example, to fabricate SP-CPB/SP-CPI NHSs, we employed spin coating technique as illustrated in Fig. S3 (ESI†). SP-CPB dissolved in toluene were spin coated onto a glass substrate followed by thermal annealing at 60 °C for 10 minutes. Subsequently, a SP-CPI film was deposited on top of it and annealed to complete the formation of SP-CPB/SP-CPI NHSs. For long term PL studies, a thin film of poly methylmethacrylate (PMMA) was spin coated on top of the heterostructure to protect the CPI from moisture, as it is prone to degradation under ambient conditions.[36,39] In a similar manner, we fabricated the MS-CPB/MS-CPI NHSs, in which smaller PbSe islands are present on the perovskite surface. The PXRD patterns and their cross-sectional field-emission scanning electron microscopy (FESEM) are given in Fig. S4 and S5 (ESI†). These results suggest that both the perovskite layers maintain their distinct stoichiometry, without any halide mixing which would otherwise lead to the formation of mixed alloys. Optical studies confirm the protective role of PbSe decoration on perovskite NCs in sufficiently inhibiting the ion exchange reaction within CPB/CPI NHSs. Fig. 2a shows the absorption and PL emission for pristine CPB and CPI NCs exhibiting emission in the green and

 This journal is © The Royal Society of Chemistry 2024

Published on 15 mai 2024. Downloaded on 15.11.2025 00:31:20.

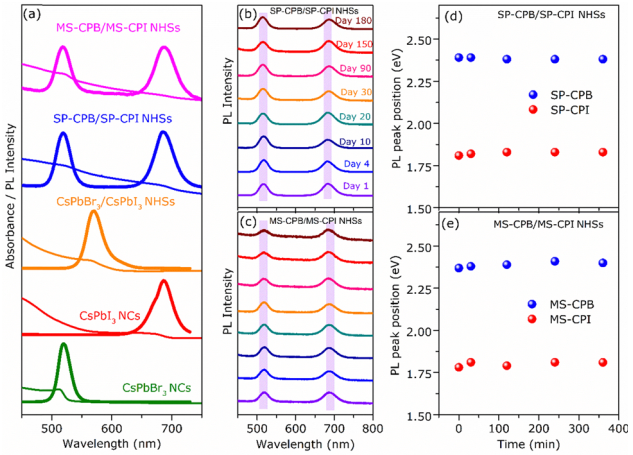

Fig. 2 (a) Absorbance and PL spectra of films of CPB, CPI, CPB/CPI and SP/MS-CPB/CPI NHSs deposited sequentially; (b) and (c) PL of the SP-CPB/SP-CPI and MS-CPB/MS-CPI NHSs over the course of six months; evolution of emission peak position with time upon heating at 100 °C of (d) SP-CPB/SP-CPI; and (e) MS-CPB/MS-CPI NHSs.

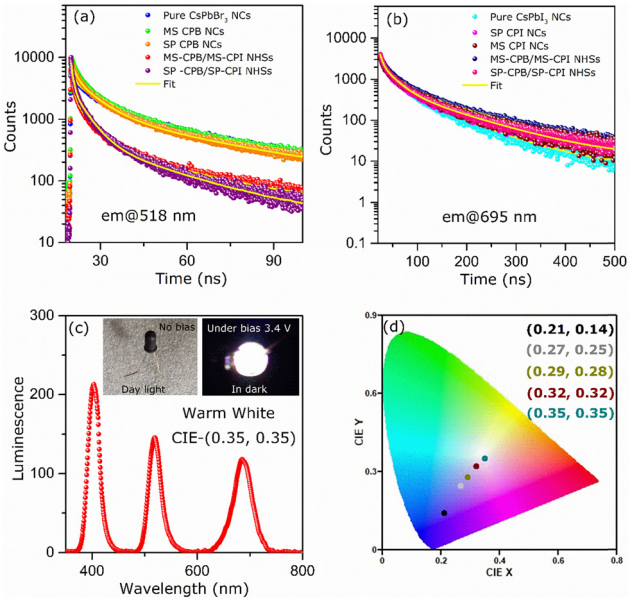

Fig. 3 TRPL decay curves of (a) pristine CPB, SP/MS-CPB, and their corresponding NHSs; (b) pristine CPI, SP/MS-CPI, and their corresponding NHSs; (c) PL spectra of pc-LED fabricated by stacking SP-CPB and SP-CPI on 405 nm emitting commercial LED. Inset shows photographs of the LED without and with applied bias of 3.4 V; (d) CIE plot for LEDs fabricated with different proportions of SP-CPB:SP-CPI.

red regions, respectively. Upon NHSs formation the absorption onset and PL emission rapidly merge within 10 minutes – the time required for thin film preparation – displaying an excitonic peak at 564 nm and emission centred at 570 nm. This aligns with expectations when the halides mix together and form $CsPb(Br_{1.5}I_{1.5})$.[18,22] On the contrary, in the SP/MS-CPB/CPI NHSs, distinct absorbance and PL features persist resembling those of isolated samples. Anion exchange in solution occurs at a much faster rate though, as seen in Fig. S6 (ESI†). The distinct absorption and emission features in films provide compelling evidence that no anion exchange occurs in the presence of PbSe in the NHSs, irrespective of the size of the PbSe domain.[46] The emission spectra of the PbSe decorated CPB/CPI tandem architecture were recorded for a period of six months without any discernible shift in the peaks for the SP/MS-NHSs as shown in Fig. 2b and c. Their absorption spectra are also unaffected as shown in Fig. S7 (ESI†). PXRD results shown in Fig. S8 (ESI†) also support the optical results. This indicates the stability of PbSe decorated heterostructures towards ion exchange reactions under ambient conditions. Halide interdiffusion across the SP/MS-CPB/CPI NHSs was also monitored at higher temperature (100 °C) by tracking the change in PL spectra with time. The evolution of PL emissions upon heating at 100 °C are depicted in Fig. S9a and b (ESI†) for SP-CPB/SP-CPI NHSs and MS-CPB/MS-CPI NHSs, respectively, and the changes in the emission peaks with time at 100 °C are shown in the Fig. 2d and e for both SP and MS based NHSs, respectively indicating no halide mixing. Heating, however, does have detrimental effects on the perovskite structure as evident from the prolonged heating at 100 °C. To understand the charge carrier dynamics within SP-CPB/SP-CPI and MS-CPB/MS-CPI NHSs, we conducted time-resolved photoluminescence (TRPL) measurements. All the measurements were performed on glass substrates. Fig. 3a and b show the decay dynamics for the emission centred at 518 nm and 695 nm, respectively. The results are fitted well with triexponential components and are summarized in Tables S1 and S2 in ESI.† Interestingly, the addition of PbSe to $CsPbX_3$ NCs has resulted in a slightly slower PL decay. This effect is ascribed to the surface defect passivation in the perovskite, resulting from the presence of PbSe islands. Upon formation of MS/SP-CPB/CPI NHS films, carriers within CPB exhibit faster decay compared to the pure sample as seen in Fig. 3a while carriers within CPI, when incorporated into the heterostructure, demonstrate slightly slower decay relative to the pure CPI as evidenced from Fig. 3b, suggesting photogenerated carriers can easily be transferred from CPB to CPI. This is in agreement with the type-I band alignment of CPB/CPI, enabling the charge carriers to flow from CPB to CPI NCs.[36] Energy is funnelled from the higher band gap CPB to the lower band gap CPI layers and at the same time retaining the identities of the two layers. To demonstrate the applicability of these NHSs, we fabricated proof-of-concept phosphor converted LEDs (pc-LEDs) with SP-CPB/SP-CPI NHSs.[21,47–49] Both the SP-CPB and SP-CPI NCs were deposited on top of a commercially available violet emitting LED (405 nm). On applying voltage of 3.4 V and 0.1 mA current, we observe white light emission from the pc-LED – the blue part emanating from the LED, green from the SP-CPB layer while red originates from the SP-CPI layer. The spectrum of the LED is shown in Fig. 3c. This is made possible because of the non-mixing of halides, confirming the effectiveness of the PbSe islands in blocking the halide migration. The amount of the two NCs can be varied to achieve various shades of white light ranging between cool white and warm white. The inset in Fig. 3c shows the photographs of the pc-LEDs in OFF state under day light and with bias in dark, illustrating warm white emission. The corresponding CIE chromaticity coordinates diagram is shown in

Published on 15 mai 2024. Downloaded on 15.11.2025 00:31:20.

Fig. 3d exhibiting the tuning of different hues of white at different ratios of SP-CPB and SP-CPI represented by CIE coordinates in Fig. 3d.

In conclusion, we have demonstrated a new approach to prevent the anion migration at the interface of $CsPbBr_3/CsPbI_3$ NHSs *via* decorating the perovskites with PbSe islands. This is a consequence of the halide vacancies being populated with the chalcogenide anion, thus making a stronger, stabler covalent bonding that prevents migration for months. The stable perovskite NCs enable us to demonstrate pc-LEDs. Further light energy harvesting applications should also be possible.

S. K. is thankful to IIT Delhi for the research fellowship. P. Y. is thankful to CSIR for the research fellowship. S. S. acknowledges CRF and SATHI, IIT Delhi for TEM and TRPL facilities and SERB, DST grant no. CRG/2019/000935, for partial financial assistance.

Conflicts of interest

There are no conflicts to declare.

Notes and references

1 S. Bera and N. Pradhan, *ACS Energy Lett.*, 2020, **5**, 2858–2872.
2 S. Khurana, M. S. Hassan, P. Yadav, D. Ghosh and S. Sapra, *J. Phys. Chem. Lett.*, 2022, **13**, 2591–2599.
3 R. S. Lamba, P. Basera, S. Bhattacharya and S. Sapra, *J. Phys. Chem. Lett.*, 2019, **10**, 5173–5181.
4 A. Chakrabarty, S. Satija, U. Gangwar and S. Sapra, *Chem. Mater.*, 2020, **32**, 721–733.
5 J. Hao, Y.-H. Kim, S. N. Habisreutinger, S. P. Harvey, E. M. Miller, S. M. Foradori, M. S. Arnold, Z. Song, Y. Yan, J. M. Luther and J. L. Blackburn, *Sci. Adv.*, 2021, **7**, 18.
6 R. M. Kennard, C. J. Dahlman, H. Nakayama, R. A. Decrescent, J. A. Schuller, R. Seshadri, K. Mukherjee and M. L. Chabinyc, *ACS Appl. Mater. Interfaces*, 2019, **11**, 25313–25321.
7 C. R. Roy, D. Pan, Y. Wang, M. P. Hautzinger, Y. Zhao, J. C. Wright, Z. Zhu and S. Jin, *J. Am. Chem. Soc.*, 2021, **143**, 5212–5221.
8 R. S. Lamba, P. Basera, S. Singh, S. Bhattacharya and S. Sapra, *J. Phys. Chem. C*, 2021, **125**, 1954–1962.
9 A. Singh, R. S. Lamba, S. Kumar and S. Sapra, *J. Phys. Chem. C*, 2022, **127**, 468–475.
10 P. Yadav, S. Khurana, R. S. Lamba, S. Singh, V. Jha, S. Kumar and S. Sapra, *Adv. Opt. Mater.*, 2024, **2302456**, 1–7.
11 P. Schulz, D. Cahen and A. Kahn, *Chem. Rev.*, 2019, **119**, 3349–3417.
12 A. Kojima, K. Teshima, Y. Shirai and T. Miyasaka, *J. Am. Chem. Soc.*, 2009, **131**, 6050–6051.
13 M. M. Lee, J. Teuscher, T. Miyasaka, T. N. Murakami and H. J. Snaith, *Science*, 2012, **338**, 643–647.
14 J. S. Manser, J. A. Christians and P. V. Kamat, *Chem. Rev.*, 2016, **116**, 12956–13008.
15 P. Yadav, D. Gill, S. Khurana, R. S. Lamba, S. Bhattacharya and S. Sapra, *J. Phys. Chem. C*, 2022, 2–11.
16 P. Yadav, S. Khurana and S. Sapra, *Nanotechnology*, 2022, **33**, 415706.
17 C. Eames, J. M. Frost, P. R. F. Barnes, B. C. O'Regan, A. Walsh and M. S. Islam, *Nat. Commun.*, 2015, **6**, 2–9.
18 A. Haque, T. D. Chonamada, A. B. Dey and P. K. Santra, *Nanoscale*, 2020, **12**, 20840–20848.
19 A. Sadhanala, S. Ahmad, B. Zhao, N. Giesbrecht, P. M. Pearce, F. Deschler, R. L. Z. Hoye, K. C. Gödel, T. Bein, P. Docampo, S. E. Dutton, M. F. L. De Volder and R. H. Friend, *Nano Lett.*, 2015, **15**, 6095–6101.
20 T. Elmelund, R. A. Scheidt, B. Seger and P. V. Kamat, *ACS Energy Lett.*, 2019, **4**, 1961–1969.
21 C. Guhrenz, A. Benad, C. Ziegler, D. Haubold, N. Gaponik and A. Eychmüller, *Chem. Mater.*, 2016, **28**, 9033–9040.
22 P. V. Kamat and M. Kuno, *Acc. Chem. Res.*, 2021, **54**, 520–531.
23 N. T. Shewmon, H. Yu, I. Constantinou, E. Klump and F. So, *ACS Appl. Mater. Interfaces*, 2016, **8**, 33273–33279.
24 E. T. Hoke, D. J. Slotcavage, E. R. Dohner, A. R. Bowring, H. I. Karunadasa and M. D. McGehee, *Chem. Sci.*, 2015, **6** 613–617.
25 E. Akriti, S. B. Shi, J. Shiring, C. L. Yang, B. Atencio-Martinez, X. Yuan, Y. Hu, B. P. Gao, A. J. Finkenauer, Y. Pistone, P. Yu, B. M. Liao Savoie and L. Dou, *Nat. Nanotechnol.*, 2021, **16** 584–591.
26 M. Imran, B. T. Mai, L. Goldoni, M. Cirignano, H. B. Jalali, F. Di Stasio, T. Pellegrino and L. Manna, *ACS Energy Lett.*, 2021, **6**, 2844–2853.
27 D. Pan, Y. Fu, J. Chen, K. J. Czech, J. C. Wright and S. Jin, *Nano Lett.*, 2018, **18**, 1807–1813.
28 Q. A. Akkerman, V. D'Innocenzo, S. Accornero, A. Scarpellini, A. Petrozza, M. Prato and L. Manna, *J. Am. Chem. Soc.*, 2015, **137**, 10276–10281.
29 K. Sakhatskyi, R. A. John, A. Guerrero, S. Tsarev, S. Sabisch, T. Das, G. J. Matt, S. Yakunin, I. Cherniukh, M. Kotyrba, Y. Berezovska, M. I. Bodnarchuk, S. Chakraborty, J. Bisquert and M. V. Kovalenko, *ACS Energy Lett.*, 2022, **7**, 3401–3414.
30 K. Sandeep, K. Padmakumar, K. U. Ambili, P. Jishnu, K. H. Fousia, A. R. Ramesh, J. P. Rappai, V. Santhi and M. Shanthil, *Phys. Status Solidi B*, 2022, **259**, 1–8.
31 Z. Xu, L. Wang, Q. Han, Y. Kamata and T. Ma, *ACS Appl. Mater. Interfaces*, 2020, **12**, 12867–12873.
32 J. Pan, Y. Shang, J. Yin, M. De Bastiani, W. Peng, I. Dursun, L. Sinatra, A. M. El-Zohry, M. N. Hedhili, A.-H. Emwas, O. F. Mohammed, Z. Ning and O. M. Bakr, *J. Am. Chem. Soc.*, 2017, **140**, 562–565.
33 X. Zhang, L. Lv, L. Ji, G. Guo, L. Liu, D. Han, B. Wang, Y. Tu, J. Hu, D. Yang and A. Dong, *J. Am. Chem. Soc.*, 2016, **138**, 3290–3293.
34 A. Pan, M. Jurow, Y. Zhao, F. Qiu, Y. Liu, J. Yang, J. J. Urban, L. He and Y. Liu, *Nanoscale*, 2017, **9**, 17688–17693.
35 A. Loiudice, M. Strach, S. Saris, D. Chernyshov and R. Buonsanti, *J. Am. Chem. Soc.*, 2020, **141**, 8254–8263.
36 M. P. Hautzinger, E. K. Raulerson, S. P. Harvey, T. Liu, D. Duke, X. Qin, R. A. Scheidt, B. M. Wieliczka, A. J. Phillips, K. R. Graham, V. Blum, J. M. Luther, M. C. Beard and J. L. Blackburn, *J. Am. Chem. Soc.*, 2023, **145**, 2052–2057.
37 V. K. Ravi, R. A. Scheidt, A. Nag, M. Kuno and P. V. Kamat, *ACS Energy Lett.*, 2018, **3**, 1049–1055.
38 A. Pasha, P. Pramanik, J. K. George, N. Dhiman, H. Zhang, S. Sidhik, F. Mandani, S. Ranjan, A. T. Nagaraja, S. Umapathy, A. D. Mohite and R. G. Balakrishna, *ACS Energy Lett.*, 2023, 3081–3087.
39 R. Rathod, S. Kapse, D. Pal, M. R. Das, R. Thapa and P. K. Santra, *Chem. Mater.*, 2024, **36**, 1719–1727.
40 X. Zhang, M. Lu, Y. Zhang, H. Wu, X. Shen, W. Zhang, W. Zheng, V. L. Colvin and W. W. Yu, *ACS Cent. Sci.*, 2018, **4**, 1352–1359.
41 J. Zhang, X. Liu, P. Jiang, H. Chen, Y. Wang, J. Ma, R. Zhang, F. Yang, M. Wang, J. Zhang and G. Tu, *Nano Energy*, 2019, **66**, 104142.
42 X. Zhang, X. Wu, X. Liu, G. Chen, Y. Wang, J. Bao, X. Xu, X. Liu, Q. Zhang, K. Yu, W. Wei, J. Liu, J. Xu, H. Jiang, P. Wang and X. Wang, *J. Am. Chem. Soc.*, 2020, **142**, 4464–4471.
43 S. Wang, C. Bi, A. Portniagin, J. Yuan, J. Ning, X. Xiao, X. Zhang, Y. Y. Li, S. V. Kershaw, J. Tian and A. L. Rogach, *ACS Energy Lett.*, 2020, **5**, 2401–2410.
44 M. Jagadeeswararao, P. Vashishtha, T. J. N. Hooper, A. Kanwat, J. W. M. Lim, S. K. Vishwanath, N. Yantara, T. Park, T. C. Sum, D. S. Chung, S. G. Mhaisalkar and N. Mathews, *J. Phys. Chem. Lett.*, 2021, **12**, 9569–9578.
45 L. Protesescu, S. Yakunin, M. I. Bodnarchuk, F. Krieg, R. Caputo, C. H. Hendon, R. X. Yang, A. Walsh and M. V. Kovalenko, *Nano Lett.*, 2015, **15**, 3692–3696.
46 S. Khurana, M. S. Hassan, P. Yadav, T. D. Chonamada, M. R. Das, P. K. Santra, D. Ghosh and S. Sapra, *J. Phys. Chem. C*, 2023, **127**, 3355–3366.
47 S. Sapra, S. Mayilo, T. A. Klar, A. L. Rogach and J. Feldmann, *Adv. Mater.*, 2007, **19**, 569–572.
48 M. Ali, S. Chattopadhyay, A. Nag, A. Kumar, S. Sapra, S. Chakraborty and D. D. Sarma, *Nanotechnology*, 2007, **18**, 075401.
49 U. Soni, A. Pal, S. Singh, M. Mittal, S. Yadav, R. Elangovan and S. Sapra, *ACS Nano*, 2014, **8**, 113–123.

 This journal is © The Royal Society of Chemistry 2024